Parameter estimation for a global tide and surge model with a memory-efficient order reduction approach

Wang, Xiaohui; Verlaan, Martin; Apecechea, Maialen Irazoqui; Lin, Hai Xiang

Citation (APA)
Wang, X., Verlaan, M., Apecechea, M. I., & Lin, H. X. (2022). Parameter estimation for a global tide and surge model with a memory-efficient order reduction approach. *Ocean Modelling*, *173*, Article 102011. https://doi.org/10.1016/j.ocemod.2022.102011

Important note
To cite this publication, please use the final published version (if applicable).
Please check the document version above.

Check for updates

Parameter estimation for a global tide and surge model with a memory-efficient order reduction approach

Xiaohui Wang [a,*], Martin Verlaan [a,b], Maialen Irazoqui Apecechea [b], Hai Xiang Lin [a]

[a] *Delft Institute of Applied Mathematics, Delft University of Technology, Mekelweg 4, 2628 CD, Delft, The Netherlands*
[b] *Deltares, P.O. Box 177, Delft, 2600 MH, The Netherlands*

ARTICLE INFO

ABSTRACT

Accurate parameter estimation for the Global Tide and Surge Model (GTSM) benefits from observations with long time-series. However, increasing the number of measurements leads to a large computation demand and increased memory requirements, especially for the ensemble-based methods that assimilate the measurements at one batch. In this study, a memory-efficient parameter estimation scheme using model order reduction in time patterns is developed for a high-resolution global tide model. We propose using projection onto empirical time-patterns to reduce the model output time-series to a much smaller linear subspace. Then, to further improve the estimation accuracy, we introduce an outer-loop, similar to Incremental 4D-VAR, to evaluate model-increments at a lower resolution and subsequently reduce the computational cost. The inner-loop optimizes parameters using the lower-resolution model and an iterative least-squares estimation algorithm called DUD. The outer-loop updates the initial output from the high-resolution model with updated parameters from the converged inner-loop and then restarts the inner-loop. We performed experiments to adjust the bathymetry with observations from the FES2014 dataset. Results show that the time patterns of the tide series can be successfully projected to a lower dimensional subspace, and memory requirements are reduced by a factor of 22 for our experiments. The estimation is converged after three outer iterations in our experiment, and tide representation is significantly improved, achieving a 34.5% reduction of error. The model's improvement is not only shown for the calibration dataset, but also for several validation datasets consisting of one year of time-series from FES2014 and UHSLC tide gauges.

1. Introduction

The risk from coastal flooding generally increases due to the sea level rise and climate changes (Jongman et al., 2012; Muis et al., 2017). The sea level can reach especially high values where tidal amplitudes are large. It is even more destructive, especially when the storm surge coincides with the high-water during spring tide (Pugh, 1996). Hydrodynamic tide and storm-surge models play an important role in assessments of flood risk and sea level rise and for forecasting. Extreme sea levels are often a combination of high tides and a storm surge. The accuracy of the reproduction of both tides and storm surge is important for these applications (Ward et al., 2015). In deep water, tides and storm surge can be modeled independently, but in shallow water non-linear interactions are more prominent. With the future aim to model these interactions, we develop a combined global tide and surge model (GTSM). However, this paper focuses on the tides and considers tides separately. Stammer et al. (2014) summarized the developments in global tide modeling and compared a number of global

tide models regarding their physical processes, grid resolution and so on. There are still a number of sources of model errors remaining, such as neglected physics in the model formulation, uncertainty parameters (e.g., bathymetry, bottom friction, and internal tides friction) that are not accurately known. Data assimilation is a promising approach for reducing parameter uncertainties with available observation data, e.g., altimeter and tide gauge measurements. Several successful applications of data assimilation for improving tide model performance have been reported in literatures (Edwards et al., 2015) with the adjoint methods (Das and Lardner, 1991; Bannister, 2017; Heemink et al., 2002; Zaron, 2019), and ensemble methods (Barth et al., 2010; Mayo et al., 2014; Ngodock et al., 2016; Zijl et al., 2013). In a comparison of several assimilative and non-assimilative models, Stammer et al. (2014) reported that data assimilation can contribute significantly to the accuracy of global tide models.

In our previous study, we proposed a computation-efficient parameter estimation scheme to estimate bathymetry for a high-resolution Global Tide and Surge Model (GTSM) (Wang et al., 2021). GTSM is a 2D

---

tide and surge model with an unstructured grid. The model is running operationally to forecast storm surges worldwide. Another application of GTSM is the assessment of flood risks and the potential impacts of sea level rise to extreme storm tides (Verlaan et al., 2015). In Wang et al. (2021), after the parameter estimation tide representation in GTSM was improved significantly using an ensemble type algorithm without the adjoint called DUD (Ralston and Jennrich, 1978). DUD (Does not use derivative) is a derivative-free calibration algorithm that works in an iterative way. In the estimation procedure, observation is compared with the model output in the time series formula. Tidal constituents are widely used as model output in estimation applications, such as the estimation of the FES model (Lyard et al., 2021). But tidal constituents cannot be directly computed in GTSM because GTSM is a time-stepping model. The Time-stepping model allows a more accurate representation of non-linear interactions at the coast, which is also recognized by Lyard et al. (2021). To obtain accurate tidal analysis results, we have to simulate the GTSM for a year based on the Rayleigh criterion to separate diurnal constituent S1 from K1. If one would include seasonal constituents SA and SSA, several years would be required since they show large inter-annual variability. Harmonic analysis needs a careful consideration of which tidal constituents to be included. When the length of the time-series is not an integer multiple of the period given by the frequency difference of two constituents, or a large non-integer value, then the estimation is potentially poorly conditioned, and the estimates will influence each other. In contrast, the proposed time-series POD method will produce accurate orthogonal approximations without any user intervention and regardless of the length of the time-series. In addition, hundreds of model runs would be simulated in the estimation process. Therefore, parameter estimation in tidal constituents is not feasible with the computational facilities available to us. The use of time series for weeks or a month can significantly reduce the simulation time and computational complexity. But the simulation time length of two weeks (one spring–neap cycle) is short and leads to estimates that over-fit the data to some extent (Wang et al., 2021). However, longer time series imply larger memory requirements in the analysis step, which is not feasible for the current implementation and computational cluster. Therefore, an efficient approach has to designed which can reduce the memory requirement and enable a longer simulation time length.

For ensemble-based data assimilation methods (Evensen, 1994), the memory use is proportional to the number of measurements assimilated in one batch multiplied by the number of perturbed model runs, called ensemble members. This also applies to the method used in this paper. Observations are often assimilated in one batch to maintain consistency between the estimated parameters and model output after the estimation (Evensen and van Leeuwen, 2000; Emerick and Reynolds, 2013), which cannot be guaranteed for incremental assimilation in smaller batches. However, this leads to a large size of the linearized model outputs $O(NN_tN_s)$, where N, N_t, N_s are the number of ensembles, number of observation time steps, and number of locations, respectively. When we attempt to include more observations and to estimate more parameters, this can result in a huge memory usage on a single compute-node. There are at least two ways to ease the huge memory usage problem: 1. parallelization of the linear solver; and 2. reducing the size of the problem by approximation. Here we follow the second approach by using model order reduction methods. Note that variational methods have different characteristics in terms of memory usage.

Model Order Reduction (MOR) is a collection of methods that can be used to reduce the computational complexity of mathematical models in numerical simulations with an approximation of the original model (Antoulas et al., 2015). In this paper, we develop a new method time-POD, which aims to reduce the size of the model output, so that the memory needed for data assimilation can be reduced. The method was inspired by the Proper Orthogonal Decomposition (POD) (Chatterjee, 2000), which projects the spatial patterns of the

state onto the leading singular vectors. Here we project onto the leading singular vectors of the time patterns instead. POD is one of the MOR techniques first introduced in fluid dynamics by Lumley (1967). It was already known as the Karhunen–Loève expansion (Kosambi, 1943) in statistics, and also as Principal Component Analysis (PCA) (Jolliffe and Cadima, 2016) or Empirical Orthogonal Functions (EOF) (Monahan et al., 2009) in meteorology. POD methods (Liang et al., 2002), such as the Karhunen–Loève decomposition (KLD), PCA, and Singular Value Decomposition (SVD), have been applied in various fields such as fluid dynamics (Cazemier et al., 1998), pattern recognition (Kopp et al., 1997), and more recently in control theory and inverse problems.

MOR has been applied in both ensemble-based and variational data assimilation systems (Cane et al., 1996; Farrell and Ioannou, 2001; Beck and Ehrendorfer, 2005; Cao et al., 2007). The typical application of MOR is projected based on truncated characteristic vectors in spatial patterns of model state variables. For instance, a dual-weighted proper orthogonal decomposition (DWPOD) is proposed combining with four-dimensional variational method (4DVar) to reduce state space orders in a global shallow-water model (Daescu and Navon, 2008). Lin and McLaughlin (2014) reduced the parameter dimension by POD for an EnKF data assimilation system.

In this study, we proposed two new developments based on our previous estimation scheme (Wang et al., 2021) . Firstly, a low memory storage estimation approach is implemented using the model order reduction techniques in the time patterns. Secondly, the implementation of outer-iteration improves the estimation accuracy, the reason is to better deal with the optimization of non-linear models. Dud is an iterative smoother type estimation algorithm, the memory needed is linearly increased with the simulation time length. The total data size is in the order of $O(10^9)$ when the time length is larger than one month in this application, which leads to memory issues. Therefore, we developed a time-POD approach to reduce the dimension of the model output by projecting the time space of the model output onto a smaller subspace. The main advantage of the time-POD is that the simulation required is not restricted by the Rayleigh criterion, which normally requires a year's simulation for accurate estimation of tidal constituents. The projection reduces the memory requirements while still accurately representing the time signal for any simulation length. The required length of the time-span considered then becomes limited by other considerations. In our previous experiments, a length of two weeks leads to some over-fitting for that time period (Wang et al., 2021). In this study, we performed the time-POD calibration experiments covering the one-month simulation time span. It provides significant improvements to the model accuracy and reduce the over-fitting of data used in the estimation process.

Furthermore, parameter estimation accuracy is also affected by the calibration algorithm. The approach of using a lower resolution model in the estimation is similar to Incremental 4Dvar, and an outer loop iteration can further improve the estimation accuracy by updating the reference using a new fine resolution simulation with the updated parameters (Emerick and Reynolds, 2013; Chen and Oliver, 2013). The incremental 4D-Var method consists of nested inner-loops and outer-loops to reduce computational cost for data assimilation. It is applied successfully in the assimilation system at the ECMWF (Courtier et al., 1994; Mahfouf and Rabier, 2000; Trémolet, 2007). In this study, we use a very similar structure. Coarse Incremental Estimation (Wang et al., 2021) uses a coarser grid to represent the model increments between the initial model and model with updated parameters. The outer loop uses the high-resolution model with the updated parameters from the converged inner-loop to restart the estimation process. It is expected that this will result in a better match between the observations and the fine grid model.

In Section 2, the Global Tide and Surge Model (GTSM) is introduced. Section 3 describes the parameter estimation scheme, including the time-POD application to temporal patterns and the outer loop implementation. Section 4 describes the experiment configuration including

parameter selection, observations, model and experiments set-up. In Section 5, POD performance is evaluated by firstly analyzing the accuracy of projected and reconstructed model output and secondly, comparing the bathymetry estimation results with or without the application of MOR. We also perform a parameter estimation experiment with an extended simulation time of one month. Model validation for the year 2014 is presented in Section 6. Finally, discussions and conclusions follow in Section 7.

2. Global tide and surge model

GTSM is a depth-averaged hydrodynamic model that simulates tide and surges. It plays an important role in the Global Storm Surge Information System (GLOSSIS) to provide water level and storm surge forecasts. The model is forced by tide generating forces without any lateral boundaries. The governing equations of the model are:

$$\frac{\partial u}{\partial t} + \frac{1}{h}(\nabla \cdot (huu) - u\nabla \cdot (hu)) + f \times u$$
$$= -g\nabla(\zeta - \zeta_{EQ} - \zeta_{SAL}) + \nabla \cdot (\nu(\nabla u + \nabla u^T)) + \frac{\tau}{h}$$
$$\frac{\partial h}{\partial t} + \nabla(hu) = 0 \qquad (1)$$

where h is the total water depth, u represents the depth-averaged horizontal velocity vector, f is the Coriolis force, g is the gravitational acceleration, ν is the horizontally eddy-viscosity, ζ is the water level, ζ_{EQ} is the equilibrium tide, ζ_{SAL} refers to the self-attraction and loading effect (SAL). The term τ denotes parameterizations of the friction stress. Most of the global tide energy dissipation comes from the bottom friction, and we use Chézy quadratic formulation with the coefficient of 77 m$^{1/2}$ s^{-1} in the model. Furthermore, internal tide friction is parameterized because there is approximately 1 TW energy dissipation, about 25–30% of the total, occurring in the deep ocean through internal wave drag (Maraldi et al., 2011). GTSM can also model surge using additional wind and air pressure conditions as the model forcing (Pugh and Woodworth, 2014).

We combined different datasets for the bathymetry. EMODnet bathymetry with a resolution of about 250 m is implemented as the input of bathymetry in Europe. General Bathymetric Chart of the Ocean dataset (GEBCO 2019) with 15 arc-second resolution is used at the rest of the globe. However, there is still a large uncertainty in bathymetry even though bathymetry can be measured directly, large areas of the oceans are unsurveyed and only estimated by satellite altimetry with a much lower effective resolution of 8.9 km (Weatherall et al., 2015; Tozer et al., 2019).

An essential characteristic of Delft3D-FM is unstructured grids (Kernkamp et al., 2011). The scale of tidal components is usually more prominent in the nearshore than in the deep ocean. High resolution is required in the coastal region to provide highly accurate modeling. Pringle et al. (2021) also reported that the mesh refinement in shallow waters, where the coast and at steep topography, is important for the global accuracy of the simulated astronomical tide.

Here, we use GTSM with two different resolutions (GTSM with the coarse grid and GTSM with the fine grid hereinafter). Table 1 reports the computation time of the coarse and fine resolution models. As expected, GTSM with the fine grid has a longer computational time but more accurate tide forecasts. However, many fine model simulations needed in the parameter estimation procedure would require weeks or even months of computational time, which is unbearable.

3. Parameter estimation with model order reduction

3.1. Parameter estimation framework

We design an efficient and low-memory usage parameter estimation scheme with model order reduction for the high-resolution tide models to reduce parameter uncertainties and improve forecast accuracy. The flowchart of this parameter estimation scheme is shown in Fig. 1.

Table 1
Computation time of the coarse and fine resolution GTSM models, measured for model simulation with a time length of 45 days and using 200 cores of Intel E5 processors on the Dutch National Supercomputer Cartesius. The model simulation time step is 5 min.

Model	GTSM with the coarse grid	GTSM with the fine grid
Resolution	Deep ocean: 50 km Coastal region: 5 km;	Deep ocean: 25km Coastal Europe: 1.25 km Other coastal region: 2.5 km
Cells	2 million	4.9 million
Computational time	25 min	70 min

The basic estimation algorithm applied here is called DUD (Does not use derivatives) in a generic data-assimilation toolbox OpenDA (Ralston and Jennrich, 1978; Karri et al., 2013). It optimizes the parameters by iteratively minimizing the following cost function:

$$J(x) = \frac{1}{2}(x - x_b)^T B^{-1}(x - x_b) + \frac{1}{2}[Y - H(x)]^T R^{-1}[Y - H(x)] \qquad (2)$$

where Y is the field observation vector including all time steps in $t \in [t_1, t_{N_t}]$ and all stations $(1, \dots, N_s)$. x is the vector of parameters to be estimated, with the dimension of n. $H(x)$ is the model output vector matching observation locations for all time steps. x_b is the initial parameter vector. B and R are the background and observation error covariances, respectively. The dimension of observation Y and model output $H(x)$ in all space points and time steps is as $O(N_s \times N_t)$. The first term on the right hand of the cost function (Eqs. (2)) is the background term J_b constraining the changes to the initial parameters. The second term is the observation term J_o representing the difference between model output and observations. For the brief introduction of the DUD algorithm and parameter estimation scheme, we only describe the observation term of the cost function in the following sections.

Fig. 1 shows the flowchart of the parameter estimation scheme, connecting the components DUD, time-POD and outer-loop. DUD is implemented in the inner loop combining with the coarse-to-fine strategy and time-POD application. DUD is a Gauss–Newton similar algorithm but derivative-free. It started from the model simulation of first guesses for the parameters $x_0 = x_b$ and n simulations with each parameter perturbed as $(x_1 = x_b + \delta e_1, x_2 = x_b + \delta e_2, x_n = x_b + \delta e_n)$. Parameter is updated for an approximate linear model that fits exactly through the model output for $[x_0, x_1, \dots, x_n]$. DUD iteratively finds the parameters that minimize the sum of squares between model output and observations.

We propose to improve estimation performance while reducing the computational cost and memory requirement based on the original DUD algorithm. They are several methods developed: the coarse-to-fine strategy, model order reduction in time patterns, and introduction of outer loop iterations.

In our previous study (Wang et al., 2021), a coarse-to-fine strategy called Coarse Incremental Calibration is proposed to reduce the computational cost. It is also applied here using a coarser grid model to replace the increments between the output from the initial model and the model with modified parameters. Terms $H_f(x)$ and $H_c(x)$ are defined as the model output with the fine and coarse grid, respectively. $H_f(x)$ can be approximated with $H_f(x_b) + (H_c(x) - H_c(x_b))$, thus the cost function is represented as:

$$J_o(x) = \frac{1}{2}[Y - H_f(x_b) + H_c(x_b) - H_c(x)]^T R^{-1}[Y - H_f(x_b) + H_c(x_b) - H_c(x)] \qquad (3)$$

Therefore, GTSM with the fine grid is only simulated to generate the initial model output $H_f(x_b)$. Other simulations in the inner iterations use GTSM with the coarse grid instead, which reduces the computing time to approximately 36% of the original.

In this research, we consider reducing the dimension of the model output by MOR. The dimension of model output $[H(x_0), H(x_1), \dots,$
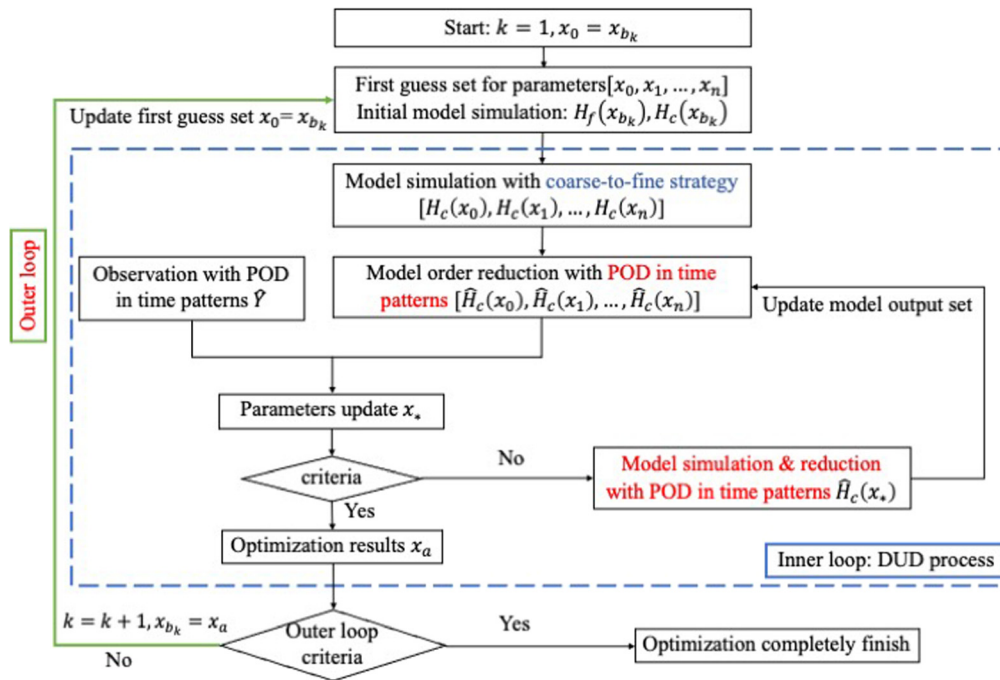
Fig. 1. Flowchart of the iterative parameter estimation scheme to connect the components: DUD, time-POD and the outer-loop iteration. New approaches we proposed in this study are in color red.

$H(x_{n+1})]$ and observations y is huge, which requires a huge memory, especially when the model has a long simulation time length. For example, if the number of observations N_s is $O(10^3)$, and with the number of time steps N_t is $O(10^3)$. Then, the dimension of the model output $H(x)$ and observations y is $O(10^6)$. If we assume the parameter dimension n is in the order of $O(10^2)$. The parameter dimension is the length of the vector with the parameters estimated. In this paper, we define spatial subdomains where a single multiplicative adjustment is applied. Each of these subdomains adds an element to the parameter vector. Thus, the dimension of the model output in the analysis step is $O(10^8)$, such a huge memory usage is unacceptable in practice. Therefore, we apply POD in the time patterns for model output and observations to reduce memory usage in the estimation procedure (that will be further explained in Section 3.2).

Moreover, we use the DUD process in the inner loop to obtain the updated parameters at a lower resolution (see Fig. 1). With the Coarse Incremental Calibration approach, high resolution GTSM only plays a role as the initial output $H_f(x_b)$ in Eqs. (3) while instead by the coarse grid model $H_c(x)$ for iterative update. Even though our previous experiments demonstrate that coarse-grid increments can well represent the fine-grid increments (Wang et al., 2021), the results after the estimation can still be significantly affected by the model with the coarse grid. Therefore, we introduce the outer loop to take the high-resolution model states into account. The updated parameters obtained from the previous converged DUD process are used as the new first guess to update the initial model output. The cost function can be rewritten as:

$$J_o(x) = \frac{1}{2}[Y - H_f(x_{b_k}) + H_c(x_{b_k}) - H_c(x)]^T$$
$$R^{-1}[Y - H_f(x_{b_k}) + H_c(x_{b_k}) - H_c(x)] \qquad (4)$$

where k is the iteration number of the outer loop, x_{b_k} is set to be the optimized parameters $x_{a_{k-1}}$ from the previous DUD process. The estimation process terminates once the cost function has converged.

Compared to the computation-efficient parameter estimation scheme we proposed in the previous study (Wang et al., 2021), the estimation scheme in this paper also contributes to memory reduction with the time-POD algorithm and estimation accuracy improvement

by the outer loop iterations. The combination of these methods gives a computation-efficient and memory-reduced parameter estimation framework.

The parameter estimation process with time-POD application and outer loops as shown in Fig. 1 can be summarized as follows:

1. Define first guess parameter set $[x_0, x_1, \dots, x_n]$.
2. Analyze initial model output $H_f(x_b), H_c(x_b)$, determine the corresponding POD reduced model output $\hat{H}_f(x_b), \hat{H}_c(x_b)$ with the truncated basis matrix U_{N_p}.
3. Convert the original observations to corresponding observation $\hat{Y}$ based on the truncated projection matrix.
4. Simulate the coarse grid model with the first guess parameter set, generate the POD reduced model states $[\hat{H}_c(x_0), \hat{H}_c(x_1), \hat{H}_c(x_2), \dots, \hat{H}_c(x_n)]$, and evaluate the cost function.
5. Find the new parameters x_* for an approximate linear model that fits exactly through the model output for $[x_0, x_1, \dots, x_n]$.
6. If the DUD stop criteria are not satisfied, then perform a model simulation with updated parameters x_* and do model order reduction for model output $\hat{H}_c(x_*)$, and return to step 5.
7. If model outputs with optimization results do not reach the outer loop stop criteria, then return to step 1 with the optimized parameters as a new first guess for the next iteration of the DUD process.
8. Output: optimal estimation of parameters x_a in the last outer loop.

3.2. Proper Orthogonal Decomposition (POD)

In this section, details of the application of POD to reduce model dimensions in time patterns are described. The time-POD reduced model is introduced first. Then, we define the corresponding observation term and error covariance. Finally, the complete parameter estimation procedure is summarized.

3.2.1. Time-POD reduced model
POD reduces the model order by identifying several modes with the most energies from a high-dimension system and uses these modes as a

lower-dimension subspace approximation. Usually, the discrete POD is derived with snapshots to find a smaller subspace for states in spatial patterns. A snapshot is the value of the model state vector at a certain time. However, the vast memory requirement in our application comes from the model output $H_f(x)$, $H_c(x)$ and observation Y, containing the data both in space and time patterns in the order of $O(N_s N_t)$. As the simulation time increases, the dimension in time scale N_t is usually much larger than that in the spatial scale N_s. Thus, reducing the order in the time patterns is crucial. In the brief description of model order reduction below, we use $H(x)$ to represent the model output without considering the model resolution in this section.

In Section 3.1, $H(x)$ is a vector representing output in one model simulation for all observation locations and time steps. To better explain the MOR applied to model output of time patterns, we rewrite the vector $H(x)$ into a two-dimensional array $H_{N_t, N_s}(x) = [h^1(x), h^2(x), \dots, h^{N_s}(x)] \in \mathbb{R}^{N_t \times N_s}$ to distinguish the time and space fields. $h^i(x)$ is the vector of model output for all time steps at the ith observation location. Now we want to find a projection matrix $K \in \mathbb{R}^{N_t \times N_t}$ from $\mathbb{R}^{N_t}$ to a smaller subspace which minimizes the error:

$$\|H_{N_t, N_s}(x) - K H_{N_t, N_s}(x)\|_2^2 = \Sigma_{i=1}^{N_s} \|h^i(x) - K h^i(x)\|_2 \quad (5)$$

where an optimal orthonormal projection matrix K is given by:

$$K = U_{N_p} U_{N_p}^T \quad (6)$$

$U_{N_p} = [u_1, u_2, \dots, u_{N_p}] \in \mathbb{R}^{N_t \times N_p}$ is an orthogonal matrix containing the N_p eigenvectors of the correlation matrix $H_{N_t, N_s} H_{N_t, N_s}^T$ corresponding to the N_p largest eigenvalues, starting from the largest eigenvalue corresponding to u_1 in decreasing order. The POD modes are the optimal ordered orthogonal matrix of basis vectors U_{N_p} in the least square sense. The truncated Singular Values Decomposition (SVD) is applied to derive the POD modes. It is the factorization of the matrix that generalizes the eigen decomposition via an extension of the polar decomposition:

$$H_{N_t, N_s}(x) = U \Sigma V^T \quad (7)$$

where, $U = [u_1, u_2, \dots, u_{N_t}] \in \mathbb{R}^{N_t \times N_t}$ and $V = [v_1, v_2, \dots, v_{N_s}] \in \mathbb{R}^{N_s \times N_s}$ are the orthogonal matrices, $\Sigma \in \mathbb{R}^{N_t \times N_s}$ is a diagonal matrix with rank r and diagonal values $\sigma_1, \sigma_2, \dots \sigma_r$ are the singular values of H_{N_t, N_s}. Therefore, a new matrix $\hat{H}_{N_p, N_s}$ can be defined by projecting the model output onto a smaller subspace using the truncated orthogonal matrices U_{N_p}, it is:

$$\hat{H}_{N_p, N_s}(x) = U_{N_p}^T H_{N_t, N_s}(x) \in \mathbb{R}^{N_p \times N_s} \quad (8)$$

We define the truncated orthogonal matrices $U_{N_p} \in \mathbb{R}^{N_t \times N_p}$ by keeping the first N_p columns of the matrix U, which correspond to the N_p modes with the highest energy of the dynamic system. In general, $\hat{H}_{N_p, N_s}(x)$ has a much smaller dimension compared to the model output $H_{N_t, N_s}(x)$, while retains the most important features. After the time-POD application, the two dimensional matrix $\hat{H}_{N_p, N_s}(x)$ is reshaped into the vector $\hat{H}(x)$ with a dimension of $O(N_p N_s)$:

$$\hat{H}(x) = \begin{bmatrix} U_{N_p}^T h^1(x) \\ U_{N_p}^T h^2(x) \\ \vdots \\ U_{N_p}^T h^{N_s}(x) \end{bmatrix} \quad (9)$$

$\hat{H}(x)$ is defined as the reduced model output vector used for the parameter estimation process.

3.2.2. Observation term conversion

In Section 3.2.1, the order of model output has been reduced to a corresponding model $\hat{H}_{N_p, N_s}(x)$ with a set of data identified on time patterns instead of the real time-series. To match the model output matrix formula, we denote a two-dimensional array $Y_{N_t, N_s} =$

$[y^1, y^2, \dots, y^{N_s}] \in \mathbb{R}^{N_t \times N_s}$ as the observation term that y^i is a vector containing time series in ith location, we have:

$$\hat{Y}_{N_p, N_s} = U_{N_p}^T Y_{N_t, N_s} \quad (10)$$

The truncated basis matrix U_{N_p} used here is from the initial model since both the model and observations have a strong resemblance to the tidal constituents in time patterns. The projection and reconstruction accuracy is further analyzed in Section 5.1.1. The reduced observation vector $\hat{Y}$ is:

$$\hat{Y} = \begin{bmatrix} U_{N_p}^T y^1 \\ U_{N_p}^T y^2 \\ \vdots \\ U_{N_p}^T y^{N_s} \end{bmatrix} \quad (11)$$

The observation error term has to be identified corresponding to the reduced observation term. We define the statistic of observation error at ith location over all time steps as follows:

$$R^i = E([y^i - E(y^i)][y^i - E(y^i)]^T) \quad (12)$$

where $E(y^i) = y_t^i$ is a vector of the truth at all discrete times at location i. The POD based observation error covariance $\hat{R}^i$ is:

$$\begin{aligned} \hat{R}^i &= E([\hat{y}^i - \hat{y}_t^i][\hat{y}^i - \hat{y}_t^i]^T) \\ &= E([U_{N_p}^T y^i - U_{N_p}^T y_t^i][U_{N_p}^T y^i - U_{N_p}^T y_t^i]^T) \\ &= U_{N_p}^T R^i U_{N_p} \end{aligned} \quad (13)$$

In this application, we assume observation error is time invariant. The covariance matrix R^j is a diagonal matrix with σ^2 as diagonal values (σ is the observation uncertainty and we set its value as $0.05m$ in this application), so $R^j = \sigma^2 I_{(N_t)}$. Therefore, after the model order reduction, the new observation error covariance for location i is $\hat{R}^j = \sigma^2 I_{(N_p)}$. $\hat{R}$ is the diagonal matrix including observation error covariance at all observation locations. We rewrite the cost function with the order reduced model output and observation terms as follows:

$$\begin{aligned} J_o(x) = \frac{1}{2} &[\hat{Y} - \hat{H}_f(x_{b_k}) + \hat{H}_c(x_{b_k}) - \hat{H}_c(x)]^T \\ &\hat{R}^{-1}[\hat{Y} - \hat{H}_f(x_{b_k}) + \hat{H}_c(x_{b_k}) - \hat{H}_c(x)] \end{aligned} \quad (14)$$

4. Experiment configuration

In this section, we describe the experiment configuration, including the parameter selection, model setup, observations, and the setup of three experiments.

4.1. Parameters with uncertainties

Bathymetry is known as the parameter with the largest uncertainties for GTSM, especially in deep oceans, compared to bottom friction and internal tides drag coefficient (Wang et al., 2021). Constrained by limited observations, computational sources, and storage memory, it is very hard to accurately estimate the bathymetry in over $O(10^6)$ grid cells. To reduce the parameter dimension, we partitioned the global ocean into 110 subdomains based on the study of tide propagation length and bathymetry sensitivity test results (Wang et al., 2021). A specified correction factor with uniform values is defined for each subdomain. The equation for adjusting the bathymetry in the subdomain $S_i, i = 1, \dots, n$ is:

$$D_j^* = (1 + [x]_i) D_j \quad for \ j \in S_i \quad (15)$$

where D_j is the bathymetry of the jth grid in the subdomain S_i and $[x]_i$ is the ith element of the parameter vector x. The initial guess for each parameter element is zero. In this study, the parameter x comprises the bathymetry correction factors in the 110 subdomains. For instance, if $[x]_1 = 0.05$, the bathymetry in region S_1 will be increased by 5%.

By assuming a constant adjusting correction factor in each subdomain, the parameter dimension is reduced to an acceptable size. Parameter uncertainties are defined as 5%.

To ensure a realistic bathymetry estimation, we impose three constraints for the experiments. Firstly, using the background term $\frac{1}{2}(x - x_b)^T b^{-1}(x - x_b)^T$ in the cost function as the weak constraint to prevent the adjusted parameter departs far away from the original values while only improving the estimate a little. Secondly, a two-degree transition area is applied between neighboring subdomains to avoid the correction factor jumps between different subdomains. Values for each grid cell in the transition areas are automatically interpolated by the model, leading to smoother correction factors around the partition boundary. Thirdly, a hard constraint of 10% is set for all parameters to ensure the changes are kept between −10% and 10%.

4.2. Model set-up

In this study, GTSM calibration is only based on the tide representation for two reasons. Firstly, it is not easy to obtain globally distributed surge observations, and the FES2014 dataset we used only provides tidal components. Secondly, surge is more sensitive to the wind and air pressure but less to the bathymetry. Wang et al. (2021) demonstrated it by comparing the surge simulation after the bathymetry estimation to the initial model with the UHSLC dataset. After the estimation, the water level forecast is improved from the higher tide forecast accuracy, and the changes of surge simulation are not significant. Thus, we use the tide representation of GTSM for bathymetry estimation. GTSM is forced by the tidal potential, with the Doodson number ranging from 57.565 to 375.575. We set the minimum threshold for the tidal spherical harmonic amplitude to 0.03 m, leading to a set of 58 tidal generating frequencies. Long-term tide components SA and SSA are removed from the tidal frequencies because they are still affected by non-gravitational influences. Estimation accuracy is strongly related to the simulation time length used in the estimation procedure. In principle, it has to be long enough, such as a month or even a year, to capture the essential tide frequencies. However, available computer memory cannot store the large amount of model output from many simulations with long simulation time lengths in the iterative optimization algorithm. A previous experiment selects one spring–neap cycle (14 days), which fits into the memory of 32 Gb on our cluster. However, experiment results showed the problem of over-fitting due to the insufficient simulation time length (Wang et al., 2021).

In the current experiments, we use a simulation time of two weeks, between 1 to 14 January 2014, to compare the estimation performance with and without the time-POD model reduction. After that, the final model estimation covers the simulation of two spring–neap cycles (1 month) with time-POD and outer loop application. Therefore, the simulation starts from 1 to 31 January 2014 with a two-week spin-up before January 1. The time interval is set as 10 min, which results in 4465 time steps.

4.3. Observation network for calibration and validation

Our parameter estimation uses the tide series derived from the FES2014 dataset in the deep ocean. Tide gauge data from the University of Hawaii Sea Level Centre (UHSLC) is applied for the model validation (Caldwell et al., 2015).

The FES2014 dataset comes from the FES (Finite Element Solution) tide model consisting of about 2.9 million nodes (Carrere et al., 2013). Long altimeter time series, tide gauges, improved modeling, and data assimilation techniques have provided an accurate solution for FES2014. FES2014 performs better than GTSM when comparing with Deep-Ocean Bottom Pressure Recorder data (Wang et al., 2021; Stammer et al., 2014). And FES2014 has an advantage in deep ocean calibration because of its ease of obtaining arbitrary time series and locations globally. Therefore, the FES2014 dataset is selected as the

Table 2
Experiments set-up.

Name	Simulation time[a]	Time steps	Outer loop	POD	Modes size	Data size before POD	Data size after POD
EX1	1–14 Jan.	2017	No	No	N/A	3.32 Gb	N/A
EX2	1–14 Jan.	2017	No	Yes	200	3.32 Gb	0.33 Gb
EX3	1–31 Jan.	4465	Yes	Yes	200	7.35 Gb	0.33 Gb

[a]Experiments are performed in the year of 2014.

observations for model calibration. 1973 time series with 32 tide constituents (excluding long-term constituents SA and SSA) are derived from the FES2014 dataset for the model calibration. These 1973 locations are almost evenly distributed in the ocean.

The UHSLC dataset is a collection of approximately 500 distributed tide gauge time series covering different years across the globe. The specific amount of available data varies over the years. Two levels of quality control, Fast Delivery (FD) and Research Quality Data (RQD), are provided in the UHSLC dataset. Tide gauges are somewhat irregularly distributed, and most of them are in the coastal regions, which leads the data more suitable for model validation than global model calibration. We retrieved the 283 tide gauge series from the hourly RQD in the year 2014. After the tide analysis with tidal analysis software (TIDEGUI) and visual inspection of the tide and surge representations against the measured series in the tide analysis procedure, tide representations with a set of 93 components from 230 tide gauge stations are finally used for the model validation.

It is worth noting that long-term tidal constituents SA and SSA are removed from FES2014 and UHSLC tide representations to ensure the consistency between observations and model output. Also, even though some tide gauge data are assimilated in the FES2014 dataset, It is still reasonable to assume that FES is independent of UHSLC data. On the one hand, most of the tide gauges are in the coastal regions, while the 1973 time series we derived are for the deep ocean. On the other hand, UHSLC data in this application is used to evaluate the estimated model performance in the coastal regions.

4.4. Experiments set-up

Three experiments are set up to investigate the performance of the time-POD parameter estimation scheme for GTSM, as Table 2 shows. EX1 is the experiment with a short simulation time of two weeks without POD implementation and the outer loop. It is very similar to the experiment in Approach 2 of Wang et al. (2021). The memory needed for the total model output in this scheme to estimate 110 parameters is approximately 3.5 Gb. EX2 has the same settings as EX1 but with the implementation of POD. It aims to evaluate the influence on the accuracy by applying POD, the memory use is significantly reduced when compared to EX1. Finally, the experiment denoted as EX3 follows the parameter estimation scheme in Fig. 1, covering a 1-month simulation time length from 1 to 31 January 2014. Without MOR, the data size of $[H_c(x_0), H_c(x_1), \ldots, H_c(x_n)]$ and observation was about 7.35 Gb, and the total memory use was more than 20 Gb for this experiment. With the proposed POD approach, the memory use is sharply reduced to 4.5% after the POD application.

5. Numerical experiments and results

To assess the performance of POD, we first evaluate the projection and reconstruction accuracy of the model output and observations, followed by a comparison of results between EX1 and EX2. At last, the estimation results in EX3 are analyzed.
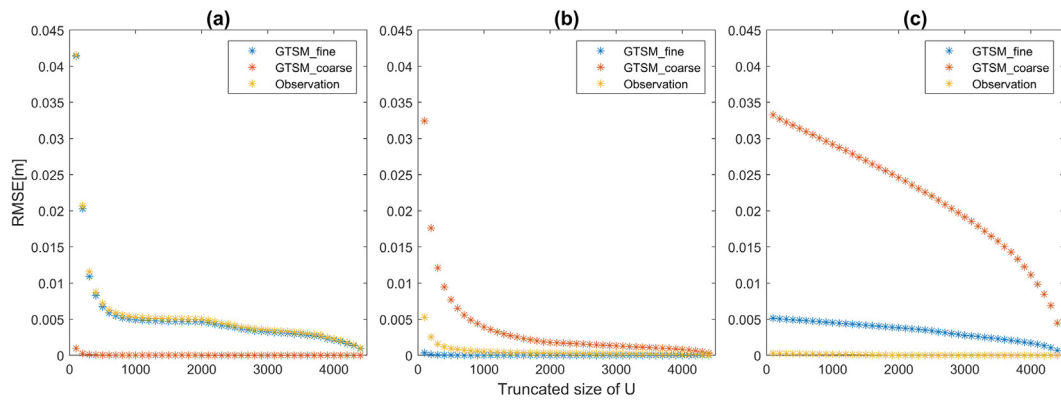
Fig. 2. RMSE between the initial model output $H(X)$ and reconstructed model output $\hat{H}(x)$ for various truncation sizes (unit: m). With the projection basis vectors derived from (a) initial coarse model; (b) initial fine model; (c) observations.
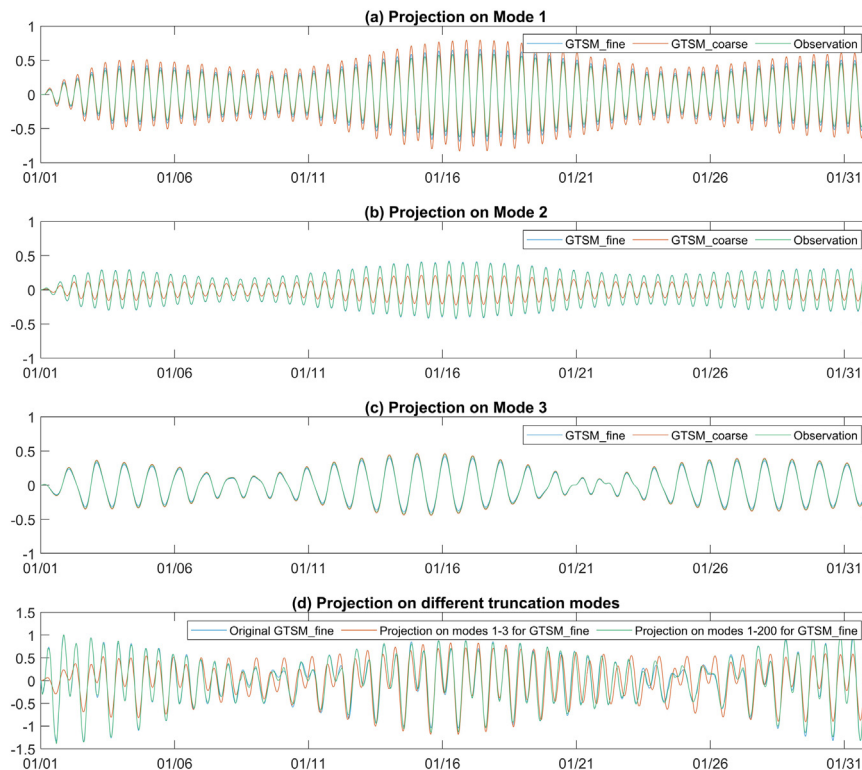

Fig. 3. Time series of the model output and observation with projection in the observation location $(-70.1110, -23.1397)$. (a) Projection on Mode 1; (b) Projection on Mode 2; (c) Projection on Mode 3; (d) Projection on different truncation modes.

5.1. POD performance analysis

5.1.1. Reconstruction accuracy

The accuracy of parameter estimation with MOR depends on the reconstruction accuracy of the model output and observations. The reconstructed model output and observation terms are in the formula of $U_{N_p} U_{N_p}^T H_{N_s,N_t}(x)$ (the term $K H_{N_s,N_t}(x)$ in Eqs. (5)) and $U_{N_p} U_{N_p}^T Y$. The basis matrix U_{N_p} is obtained by truncated SVD from the initial model output or observations. Fig. 2 shows the Root Mean Square Error (RMSE) between the original and the reconstructed model output (observation) with different number of modes. Time series is from 1 to 31 January 2014.

In general, the RMSE is decreased with the increase of the truncation size. Basis matrix from observation (Fig. 2c) shows slower downtrends than others (Fig. 2a, b). One possible reason is the model has more tidal components that are not included in the observations, there are 32 tidal constituents in observations while 58 tide potential frequencies are in

the model. But that will not affect the estimation results because the RMSE for reconstructed model and observations without truncation is less than 5×10^{-4} m. It means the missing components in observation would lead to at most 5×10^{-4} m water level changes while the observation error we defined is 0.05 m, which is 100 times larger. Fig. 2a shows the excellent accuracy of the reconstructed coarse model. The reconstructed fine model and observations have similar performance when the truncation size varies. Fig. 2b is opposite to Fig. 2a for the coarse model. We use the basis matrix from the coarse model with 200 modes for the calibration process because most of the model simulation in the estimation iteration is on the coarse grid. Reducing the coarse model output with 200 modes sharply reduces the data size, while the high accuracy for the coarse model with RMSE of 2.64×10^{-4} m is attained and the reconstructed observation error is also smaller than the observation uncertainty.

Tidal analysis can also be used to reduce the data size, but in comparison, the time-pattern projection has two advantages. Firstly, tidal
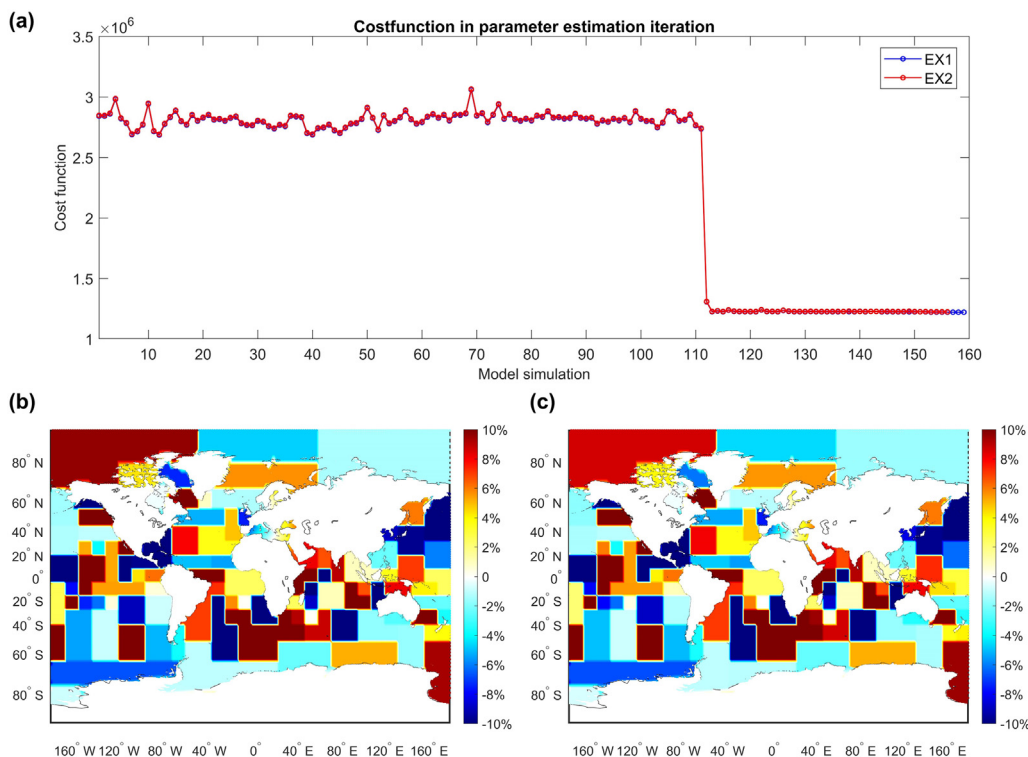
Fig. 4. (a) Cost function in EX1 and EX2. Relative adjustments of Bathymetry as estimated in EX1 (b) and EX2 (c). Positive values show a deepening.

Table 3
The amplitude of eight major tide components from tide analysis for the time-series of the original GTSM with fine grid and the projection on mode 1–3 for the arbitrary location in (cm): $(-70.1110, -23.1397)$.

Components	Q1	O1	P1	K1	N2	M2	S2	K2
GTSM with fine grid	7.2	26.06	7.18	21.89	6.34	46.74	33.73	9.58
Projection on mode 1	0.22	1.73	0.77	2.35	8.54	40.92	12.10	3.44
Projection on mode 2	0.23	0.53	0.30	0.90	5.51	26.10	8.05	2.29
Projection on mode 3	4.89	15.33	6.96	21.21	0.80	2.31	1.92	0.54

Fig. 5. RMSE difference between the initial model and estimated model in EX2 in the period from 1 to 14 January 2014, color blue shows the improvement. [unit:m].

analysis requires the selection of a set of tidal constituents. These constituents should respect the Rayleigh criterion. The projection method has only one parameter to which is quite insensitive. For example, time-series of reconstructed model output and observations for modes 1 to 3 (Fig. 3a–c) in an observation location provide similar waves to the harmonic, implying the patterns in the projection method work similarly as the tide analysis does but without the restriction to separating the independent tide components. Secondly, the projection method gives almost identical results to the time-series approach. The reconstructed fine grid model output with projection on the first three modes (Fig. 3d) is close to the original data. When more modes (200 modes we selected) are included, the reconstruction error would become very small. We also performed a tidal analysis for the time series from the model output for this location and after projection onto modes 1–3, as shown in Table 3. The projection on modes 1 and 2 mainly shows large amplitudes for the semi-diurnal tides (N2, M2, S2, K2). The contributions from N2 and M2 add up to a large part of the N2, M2 signal, while this is a bit less for S2 and K2. Mode 3 mainly shows diurnal constituents, where the P1 and K1 amplitudes are close to the values for the full signal. The time projection thus shows some resemblance to tidal analysis.

5.1.2. Experiments with time-POD application

Fig. 4 shows the cost function (Fig. 4a) and optimized bathymetry correction factors of EX1 (Fig. 4b) and EX2 (Fig. 4c). EX2, estimation with time-POD, shows a similar behavior of the cost function in each
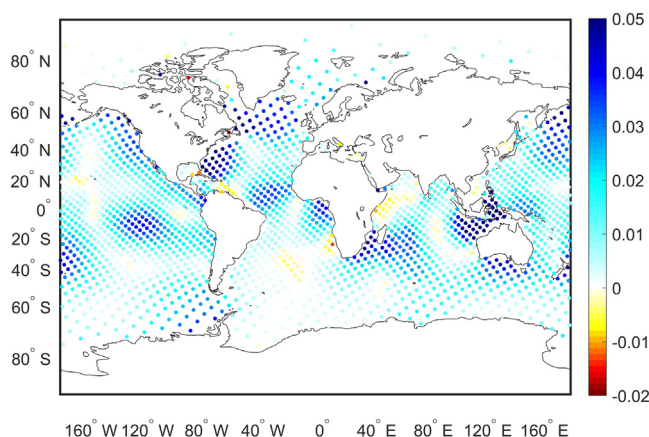
iteration as EX1 and nearly the same correction factors. The RMSE for both experiments decreases from 5.23 cm to 3.49 cm in the calibration period, while the required memory in EX2 is reduced by a factor of 10.

Fig. 5 illustrates the difference of RMSE at different observation locations between the initial model and the estimated model in EX2 (i.e., RMSE between the initial model and observations — RMSE between the estimated model and observations). It reports nearly the same improvement after the estimation as in EX1 (not shown here). Therefore, model order reduction is an efficient approach to reduce memory requirements for parameter estimation without causing any loss of estimation accuracy.

The purpose of parameter estimation is to improve the GTSM long-term forecast accuracy. However, the interaction of tidal constituents varies during different periods. For example, the RMSE between estimated model output and observations is 3.49 cm from 1 to 14 January, while the RSME in the forecast increases to 4.33 cm for the period from
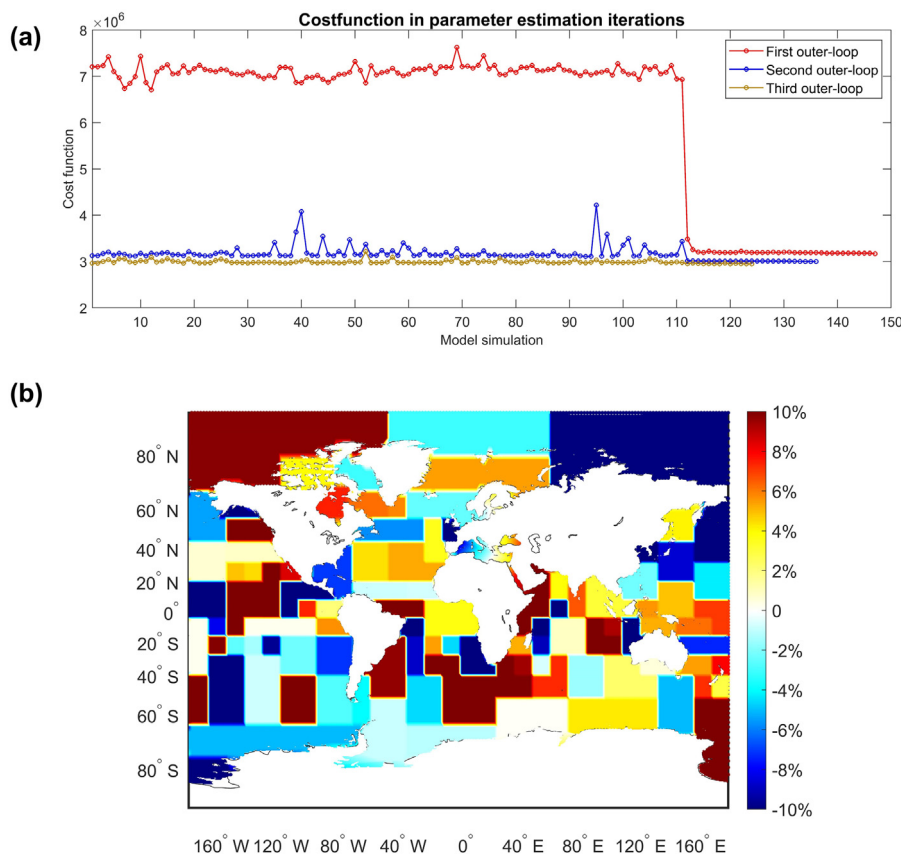
(a)

(b)

Fig. 6. (a) Changes of the cost function values in the three outer loop iterations of EX3; (b) Relative adjustments of the bathymetry as estimated in EX3; Positive values show a deepening.

15 to 31 January 2014. A short simulation time length would lead to over-fit the data in the estimation period (Wang et al., 2021). After assessing model order reduction performance, we selected a longer simulation time of 1 month and experimented in Section 5.2.

5.2. Parameter estimation results analysis

EX3 covers a simulation time length of 1 month for GTSM to estimate bathymetry. Fig. 6a illustrates the changes in the cost function in each simulation in the three outer loop iterations. In every outer loop, the cost functions of the first 111 runs include one initial simulation and 110 independent simulations each corresponding to perturbing one of the 110 parameters. Parameters are iteratively updated after the first 111 simulations. The simulation experiment was run using 200 cores for about 12 days, with a total of approximately 57 600 h CPU times.

In the first outer loop (color red in Fig. 6a), the cost function has a sharp reduction from 7.21×10^6 to 3.17×10^6 and then slowly reduced to 3.00×10^6 at the end of the second outer loop (color blue). Compared with the first outer loop, the cost function in the second outer loop only reduces slightly. It looks that the estimation results are converged to a certain value. In the third out loop, the difference of cost functions in each simulation is very slight, making the DUD process difficult to continue, leading to a stop after several iterations with a value of 2.95×10^6. It is in the same magnitude as that in the second outer loop. GTSM parameter estimation is converged in the third outer loop iteration. Moreover, sensitivity for each parameter can be observed from the variability of the cost function for the initial 111 perturbation runs in each outer loop. This is strongly decreased in the third outer loop, indicating that the estimated parameters are close to the minimum. The final relative change to the bathymetry, which is the correction factor $[x]$ in Eqs. (15) is shown in Fig. 6b. The value varies between -0.1 to 0.1 within the range of hard constraints.

Table 4
RMSE between GTSM and FE2014 datasets in difference time periods [cm].

Model	Time period	Initial	EX1	EX3_1[a]	EX3_2[a]	EX3_3[a]
GTSM with the coarse grid	1–14 Jan.	6.47	4.19	4.08	4.02	4.06
	15–31 Jan.	7.14	5.20	4.53	4.39	4.41
GTSM with the fine grid	1–14 Jan.	5.23	3.49	3.67	3.62	3.62
	15–31 Jan.	5.84	4.33	3.80	3.66	3.66

[a]EX3_1, EX3_2, and EX3_3 represent the first, second, and third outer loop.

Estimation performance is analyzed by comparing the model output with the FES2014 dataset. For the comparison of the model performance in EX3 and EX1, RMSE of two time periods is summarized in Table 4. RMSE is used to represent the difference between model output and observations to access model performance. The bias difference between model and observations is negligible (not shown here). As expected, GTSM with the fine grid has better performance than that with the coarse grid. Comparing the coarse grid GTSM, EX3 works better than EX1 in all outer loops and time periods. In the fine grid GTSM, EX1 performs slightly better than EX3 in the period 1 to 14 January but worse in 15 to 31 January 2014. This can be explained that EX1 estimates with a two-week simulation time (1 to 14 January 2014) resulting in an over-fitting of data in the calibration period. The RMSE is reduced from 5.23 cm to 3.49 cm in the period 1 to 14 January, while the reduction in the period 15 to 31 January is clearly less, from 5.84 cm to 4.33 cm in the 15 to 31 January. With a longer simulation time length of 1 month in EX3, the RMSE of the estimated fine model in these two periods is close to each other, namely 3.62 cm and 3.66 cm, implying the overfitting is reduced.

The spatial distribution of RMSE for the fine GTSM in January is shown in Fig. 7. Fig. 7a is the RMSE between the estimated fine grid
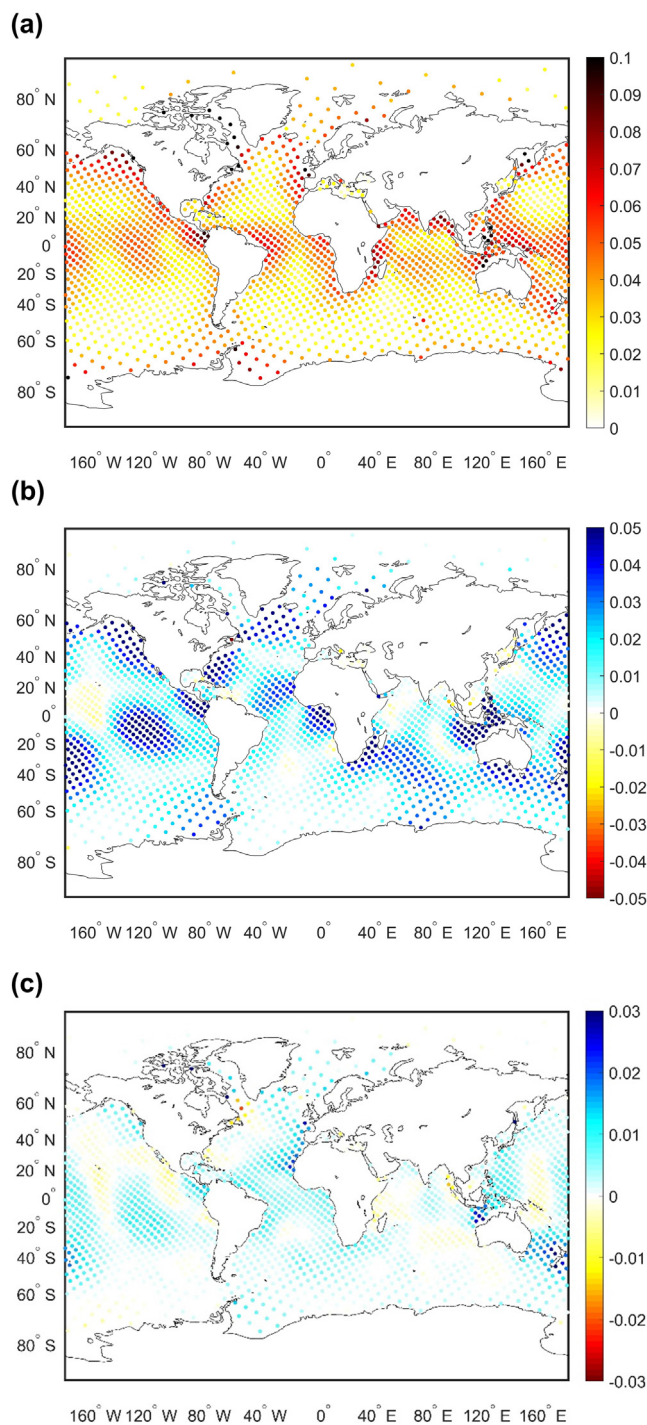
Fig. 7. (a) RMSE between estimated fine grid GTSM in EX3 and FES2014 dataset in January 2014; (b) Difference of RMSE between the initial model and the estimated model, color blue shows the improvement; (c) Difference of RMSE between model after estimation in EX1 and EX3, color blue shows EX3 outperforms EX1. [unit: m].

Table 5
RSS and RMS of eight major tide components between the fine GTSM and FES2014 dataset in (cm).

Components	RMS for all locations								RSS
	Q1	O1	P1	K1	N2	M2	S2	K2	
Initial	0.48	1.12	0.55	1.62	1.01	4.50	2.79	1.76	6.05
EX1	0.44	0.96	0.41	1.18	0.66	2.54	1.91	1.46	3.92
EX3_1	0.46	1.00	0.45	1.31	0.62	2.02	2.00	1.42	3.68
EX3_2	0.46	0.99	0.43	1.25	0.61	1.91	1.90	1.39	3.53
EX3_3	0.46	1.00	0.43	1.25	0.62	1.89	1.89	1.38	3.52

ocean; In addition, estimation by EX3 outperforms EX1 in most ocean sea, as Fig. 7c shows. Generally, the estimated model significantly overperforms the initial model.

In summary, the calibrated model in EX3 is in better agreement with the measurements than EX1. Model order reduction reduces the memory requirement by a factor of 22 while keeping a better estimation accuracy. Long simulation time is beneficial for parameter estimation in GTSM, and the implementation of the outer loop further improves the tide forecast accuracy.

6. Model validation

To validate the model performance more independently from the simulation period and data we used in the estimation procedure. We analyzed the tide components from GTSM and compared them against the FES2014 dataset in the frequency domain. The tide forecast of GTSM for the whole year of 2014 is also compared with observations from the FES2014 and UHSLC datasets.

6.1. Tide analysis comparison against FES2014 dataset for 2014

Model performance is evaluated in the frequency domain. Tide forecast from GTSM in the year 2014 for 1973 observation locations is analyzed with TIDEGUI software. We use the Root-mean-square (RMS) to assess the difference between model output and observations for major tide components, with the formula:

$$RMS = \sqrt{\overline{[(A_m cos(\omega t - \phi_m) - A_o cos(\omega t - \phi_o))]^2}} \tag{16}$$

The terms A_m and A_o are the amplitudes from model output and observations, respectively. ϕ_m, ϕ_o are terms of phases lag. ω is the tide frequency. The overbar shows the computation over one full cycle of the constituent (ωt varying from 0 to 2π) in all locations. Detailed results for 8 major tide components are summarized in Table 5. Root-sum-square (RSS) for these 8 constituents is also analyzed.

It can be observed that RSS and RMS for all 8 major components are reduced after the estimation in EX1 and three outer loop iterations of EX3 when comparing with the initial model. After the estimation, M2 is the component that significantly improved in EX3 reduced from 4.50 cm to 1.89 cm whereas it is 2.54 cm in EX1. The other 7 components in EX3 are nearly the same or slightly better than that in EX1. The RSS over these eight components in EX3 is sharply reduced from 6.05 cm to 3.52 cm.

The differences in the amplitude and phase between the model output and FES2014 dataset for M2 component are shown in Fig. 8. The difference in amplitudes and phases compared to FES2014 dataset is much smaller for the estimated models in EX1 and EX3 than for the initial model. EX3 has a better agreement with FES2014 dataset than EX1, especially in the phase domain (Fig. 8e, f), consequently EX3 has a smaller RMS than EX1.

Initial GTSM performs better in deep ocean comparing with Deep-Ocean Bottom Pressure Recorder (BPR) observation than most of the purely hydrodynamic models described in Table 3 of Stammer et al. (2014), but not as accurate as the assimilative tide models (Wang et al., 2021). In this study, GTSM is significantly improved after our
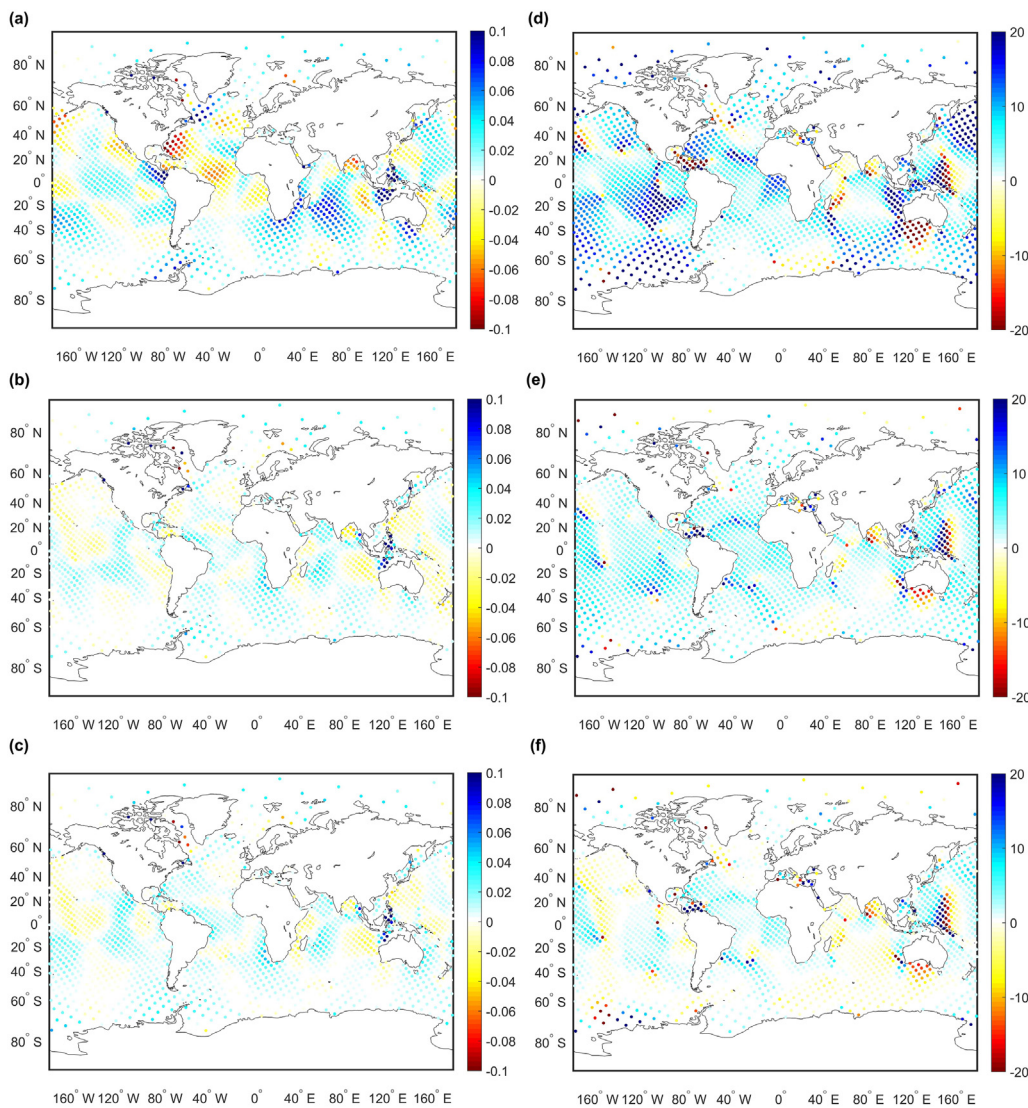
model output in EX3 and FES2014 observations. The differences of RMSE between the model before and after the estimation are shown in Fig. 7b. It can be observed that the estimated model has been significantly improved in most regions. A few areas that are not improved or a bit worse than the initial model, see the areas with yellow colors (negative values of RMSE difference) in Fig. 7b. Possibly, not only bathymetry but also other effects such as the lack of resolution, play a role here. The regions getting worse only takes up a small part of the

Fig. 8. Spatial distribution of amplitudes and phase difference of M2 between model and FES2014 dataset. (a) (b) (c): Amplitudes difference for initial GTSM, model estimated in EX1 and EX3, respectively [unit: m]. (d) (e) (f): Phases difference for initial GTSM, model estimated in EX1 and EX3, respectively [unit: degree].

parameter estimation to bathymetry in the deep ocean. It overperforms the purely hydrodynamic models, especially in the M2 constituent, but still not better than the assimilative tide models. This result is expected because firstly observation locations are limited in the estimation process, and secondly not only bathymetry but other effects such as resolutions, other parameters like bottom friction would also affect the model performance. However, compared to other tide models, GTSM after parameter estimation has the advantage to access the effect of sea level rise and climate changes because it can include surge simulation when meteorological forcing wind and air pressure additions are added. Therefore, the high accuracy tide representations also benefit the complete water level forecast.

6.2. Monthly comparison against FES2014 time series for 2014

GTSM is also validated through long-term tide forecasts, showing the model performance in different time periods. Model forecast in the whole year of 2014 is firstly analyzed with the FES2014 dataset. Fig. 9 shows the regional RMSE of the fine GTSM after the estimation in EX1 and EX3 for each month of year 2014. The regional RMSE between GTSM with the fine grid and FES2014 dataset is shown in Fig. 9a–g. The global average of RMSE in 1973 locations is shown in Fig. 9h.

Compared to the initial model, the RMSE for all the regions is significantly reduced in EX1 and EX3. RMSE in EX1 is larger than that in EX3 in the year 2014, except for some months in the Indian Ocean. Forecast results also report that estimation with a longer simulation length works better than that with a short time window when comparing the RMSE in EX1 and the first outer loop of EX3. As the number of outer loop iterations increases, the model performs better throughout 2014. The 1-year forecast comparison with the FES2014 dataset demonstrates the estimated model can be used for the high-accuracy long-term forecast.

One can also observe a seasonal pattern in the RMSE in Fig. 9, both before and after the calibration. A possible reason is that tide constituents interact differently for different periods, leading to a large or small difference between the data and the model for each month. After calibration, this seasonal pattern is smaller in EX3 than EX1, indicating long simulation time length can weaken it and result in a better agreement to model and observations. However, it remains challenging to verify whether using a more extended time period such as one year can further improve the model accuracy and eliminate over-fitting due to the excessive computational demand. But we see no clear signals of over-fitting problem in EX3, and the 1-month calibration provides sufficient calibration accuracy.
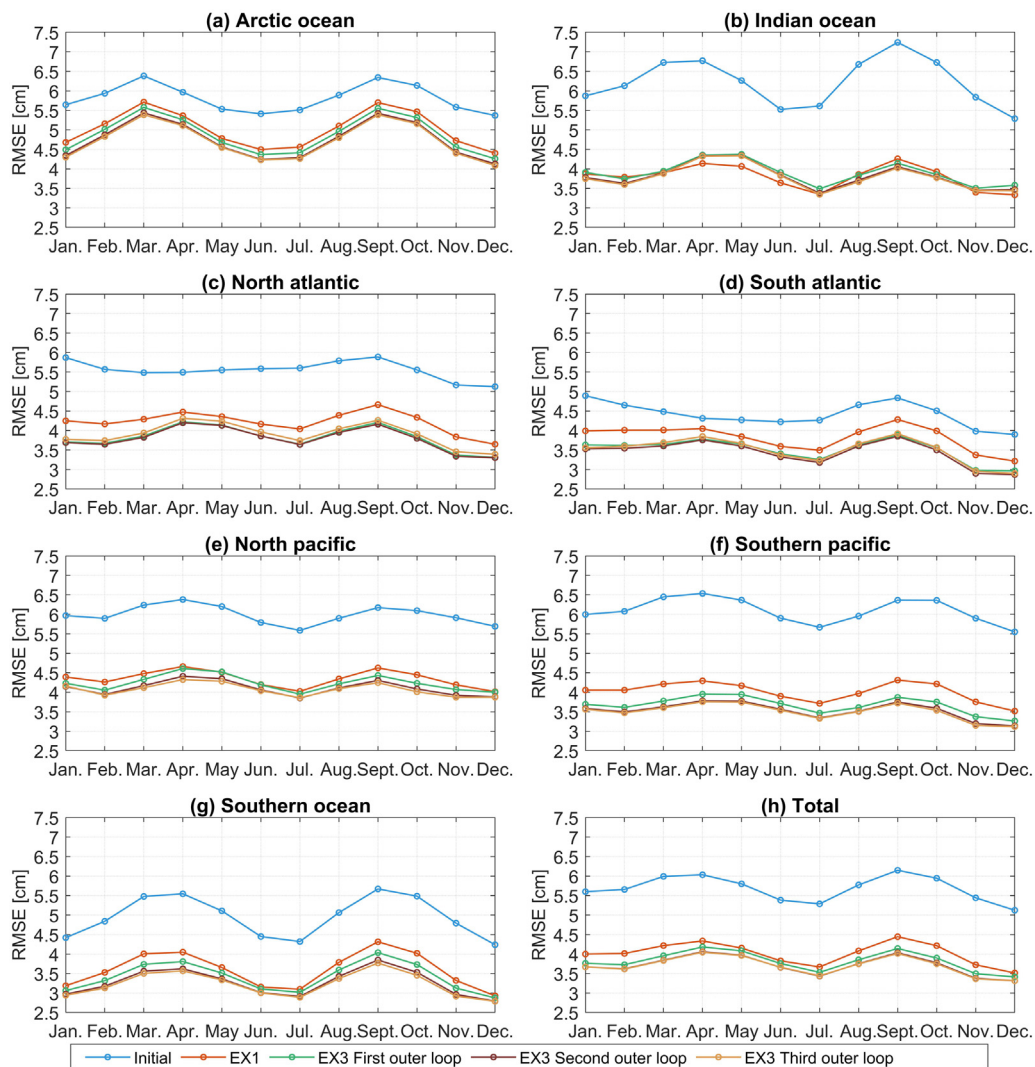
Fig. 9. Regional RMSE between GTSM with the fine grid and FES2014 dataset in2014.

6.3. Monthly comparison against UHSLC time series for 2014

In the following, the performance of GTSM is assessed using a dataset that is not used in the estimation stage. Model performance in the coastal areas is evaluated by comparing with the UHSLC dataset in 2014.

Fig. 10 shows the monthly averaged RMSE in 2014 between model output and the UHSLC measurement. The RMSE before the estimation is approximately 12.5–14 cm in each month and it is reduced to about 10–11.5 cm after the estimation in both EX1 and EX3. It indicates the bathymetry estimation for the deep ocean can improve the accuracy in the nearshore. As expected, the results in EX3 are better than in EX1. The difference between the three outer loops is not significant, but the second outer loop is slightly better than the third outer loop. It can also be observed from the mean RMSE of the whole year of 2014 (Fig. 10), the second loop has a value of 10.84 cm smaller than the third outer loop with 10.94 cm. One possible reason is the bathymetry estimation mainly works on the deep ocean. After three outer loop iterations, the parameter estimation overfits a bit the deep water observation used in the calibration process. Also, some other effects, such as bottom friction, play a role in shallow waters, but they are left out of consideration in this study. Future works can continue on the parameter estimation for shallow waters.

Fig. 11 shows the spatial distribution of RMSE between the initial fine model and UHSLC dataset in the year of 2014 (Fig. 11a) and the

RMSE difference between the model before and after estimation in EX3 (Fig. 11b). Results in EX1 reported similar distribution as EX3 but with a slightly higher RMSE (not shown here). Most of the tide gauges are located in coastal areas with larger RMSE than deep oceans. After the global calibration, model performance near the coast is improved even though the calibration mainly focuses on the deep water.

To further have a closer look at the tide representation in one location, the time series of station Wellington Harbor in New Zealand is used as an example. Fig. 12a shows the tide representation from the UHSLC dataset, the model output of the initial, EX1, and EX3. The difference between model output and observation is depicted in Fig. 12b. The RMSE for the initial model is 15.25 cm, and after the estimation in EX1, it is decreased by approximately 44.2% to 8.51 cm. EX3, with the RMSE reduction of approximately 59.21%, is marginally better than in EX1.

The model validation for the whole year of 2014 shows excellent agreement with the FES2014 and UHSLC datasets in frequency and time domains after applying the memory-efficient estimation. It illustrates that GTSM with the adjusted bathymetry can provide high accuracy long-term tide forecast.

7. Summary and conclusion

This study presented a memory-efficient parameter estimation approach for the high-resolution global tide model over a long time
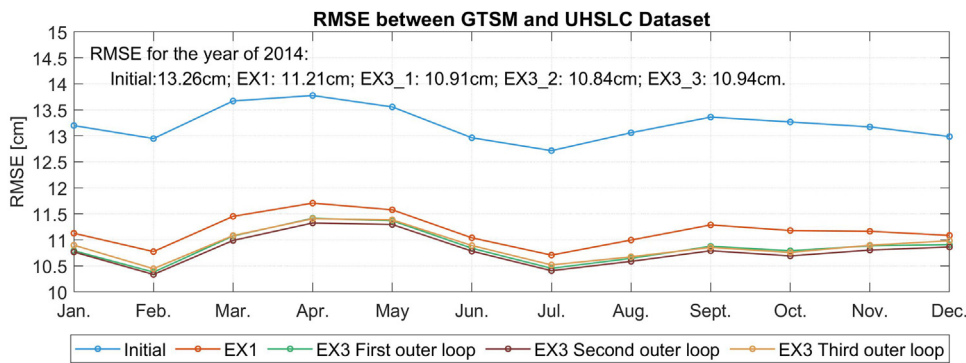
Fig. 10. RMSE between GTSM with the fine grid and UHSLC dataset in 2014.
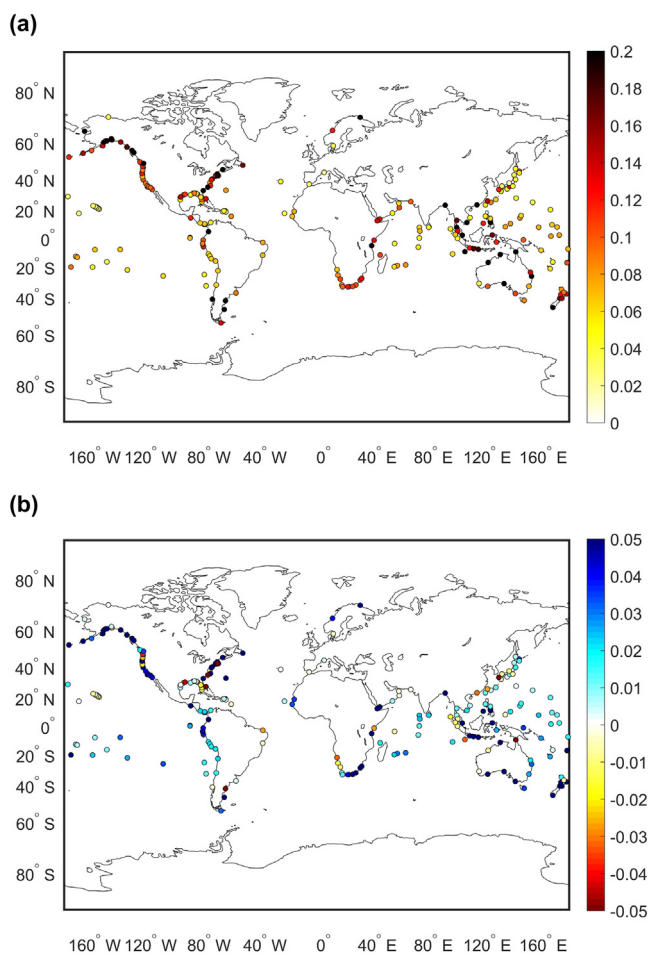

Fig. 11. (a): RMSE between initial fine GTSM and UHSLC dataset in year 2014; (b): RMSE difference between initial model and estimated model in EX3, color blue shows improvement [unit:m].

length. To resolve the memory constraint of the long period model simulation, time-POD model order reduction is developed to project the model output time patterns onto a smaller subspace. To further improve the model estimation accuracy with affordable computational cost, we implemented inner-outer loop iterations, similar to Incremental 4D-var, using an iterative parameter estimation algorithm called DUD in the inner loop with the lower-resolution model simulation. The outer loop uses optimized parameters from the previous inner DUD process

as a new reference run with the initial high-resolution model. This parameter estimation scheme is implemented for the Global Tide and Surge Model (GTSM) to correct bathymetry and substantially improve the model performance.

Our previous investigation showed that the accuracy of the calibrated model would probably benefit from a calibration period longer than the two weeks (one spring–neap cycle) used there, but the huge memory required was limiting an extension in practice (Wang et al., 2021). Here, we use time-POD model order reduction to project the GTSM output onto a limited number of time patterns. This projection reduces the memory usage by more than an order of magnitude in our experiments, while our experiments for GTSM show that parameter estimation with MOR achieves the same model accuracy as without MOR. This approach has the advantage of keeping the reduced model output size small when extending the simulation time length.

Finally, a parameter estimation experiment for GTSM with the implementation of MOR and inner-outer loop iterations is performed. It covers a simulation time of 1 month while memory demand is reduced by a factor of 22 due to model order reduction for time fields. Experiment results show that the ocean tide is better represented in the calibration period. The cost function is converged within three outer loop iterations in this study. Model validation from the frequency domains illustrates the M2 component is significantly better estimated with the set-up of 1-month simulation length and the outer loop implementation. Model tide forecast in the whole year of 2014 is compared with the FES2014 and UHSLC datasets. It demonstrates that a long simulation period in the estimation procedure improves the performance for long-term tide forecasting. The outer loop iterations contribute to further improvement of the model forecast but can lead to a bit of overfitting to the data in the third outer loop.

In summary, parameter estimation leads to significant performance improvements for GTSM. The memory requirements are significantly reduced, which allowed us to extend the time span used for calibration. This resulted in a more accurate reproduction of tides in GTSM. Bathymetry calibration contributes more to the deep ocean but also benefits a bit for shallow waters. Moreover, the time-POD parameter estimation is a general technique that can be widely used in many global or regional numerical models to estimate different parameters. Compared to harmonic analysis method, model simulation time length in time-POD estimation is not limited by the Rayleigh criterion. We have presented a case study of bathymetry estimation in a global tide and surge model. Even when only tide is simulated in the GTSM, the efficient estimation also benefits the complete water level forecasts including the tide and surge. In addition, this parameter estimation scheme can also be used to calibrate different parameters simultaneously (e.g., bathymetry, internal tide friction and bottom friction combined), in particular, to estimate the bottom friction in shallow water with more tide gauge data.
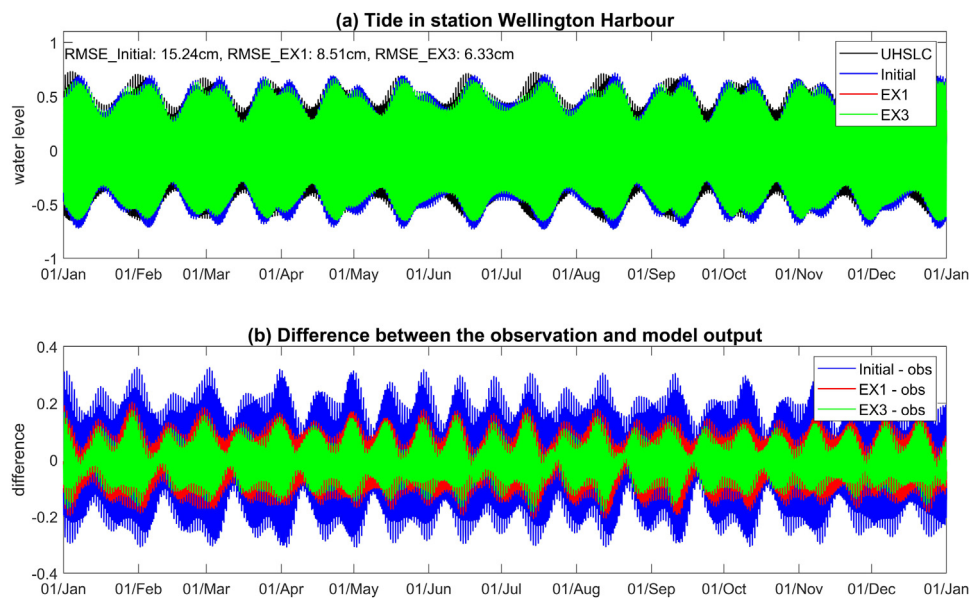
Fig. 12. (a): Tide representation for station Wellington Harbor in year 2014; (b): Difference between different GTSM models with the fine grid and observation. Wellington Harbor is a location with coordinate of (−41.28,174.78) in the New Zealand.

CRediT authorship contribution statement

Xiaohui Wang: Conceptualization, Methodology, Software, Writing – original draft. **Martin Verlaan:** Conceptualization, Writing – review & editing, Supervision. **Maialen Irazoqui Apecechea:** Software. **Hai Xiang Lin:** Writing – review & editing, Supervision.

Declaration of competing interest

The authors declare that they have no known competing financial interests or personal relationships that could have appeared to influence the work reported in this paper.

Acknowledgments

References

Antoulas, A., Ionutiu, R., Martins, N., Maten, ter, E., Mohaghegh, K., Pulch, R., Rommes, J., Saadvandi, M., Striebel, M., 2015. Model Order Reduction : Methods, Concepts and Properties. CASA-report, Technische Universiteit Eindhoven.

Bannister, R.N., 2017. A review of operational methods of variational and ensemble-variational data assimilation. Q. J. R. Meteorol. Soc. 143 (703), 607–633.

Barth, A., Alvera-Azcárate, A., Gurgel, K.-W., Staneva, J., Port, A., Beckers, J.-M., Stanev, E.V., 2010. Ensemble perturbation smoother for optimizing tidal boundary conditions by assimilation of high-frequency radar surface currents application to the german bight. Ocean Sci. 6 (1), 161–178.

Beck, A., Ehrendorfer, M., 2005. Singular-vector-based covariance propagation in a quasigeostrophic assimilation system. Mon. Weather Rev. 133 (5), 1295–1310.

Caldwell, P.C., Merrifield, M.A., Thompson, P.R., 2015. Sea Level Measured by Tide Gauges from Global Oceans – The Joint Archive for Sea Level holdings (NCEI Accession 0019568), Version 5.5. NOAA National Centers for Environmental Information, Dataset.

Cane, M.A., Kaplan, A., Miller, R.N., Tang, B., Hackert, E.C., Busalacchi, A.J., 1996. Mapping tropical Pacific sea level: Data assimilation via a reduced state space Kalman filter. J. Geophys. Res. Oceans 101 (C10), 22599–22617.

Cao, Y., Zhu, J., Navon, I.M., Luo, Z., 2007. A reduced-order approach to four-dimensional variational data assimilation using proper orthogonal decomposition. Internat. J. Numer. Methods Fluids 53 (10), 1571–1583.

Carrere, L., Lyard, F., Cancet, M., Guillot, A., Roblou, L., 2013. FES 2012: A new global tidal model taking advantage of nearly 20 years of altimetry. In: Ouwehand, L. (Ed.), 20 Years of Progress in Radar Altimatry. In: ESA Special Publication, vol. 710, p. 13.

Cazemier, W., Verstappen, R.W.C.P., Veldman, A.E.P., 1998. Proper orthogonal decomposition and low-dimensional models for driven cavity flows. Phys. Fluids 10 (7), 1685–1699.

Chatterjee, A., 2000. An introduction to the proper orthogonal decomposition. Current Sci. 78 (7), 808–817, URL: http://www.jstor.org/stable/24103957.

Chen, Y., Oliver, D.S., 2013. Levenberg–Marquardt forms of the iterative ensemble smoother for efficient history matching and uncertainty quantification. Comput. Geosci. 17, 689–703.

Courtier, P., Thépaut, J.-N., Hollingsworth, A., 1994. A strategy for operational implementation of 4D-Var, using an incremental approach. Q. J. R. Meteorol. Soc. 120 (519), 1367–1387.

Daescu, D.N., Navon, I.M., 2008. A dual-weighted approach to order reduction in 4DVAR data assimilation. Mon. Weather Rev. 136 (3), 1026–1041.

Das, S.K., Lardner, R.W., 1991. On the estimation of parameters of hydraulic models by assimilation of periodic tidal data. J. Geophys. Res.: Ocean 96, 15.

Edwards, C.A., Moore, A.M., Hoteit, I., Cornuelle, B.D., 2015. Regional ocean data assimilation. Annu. Rev. Mar. Sci. 7 (1), 21–42.

Emerick, A.A., Reynolds, A.C., 2013. Ensemble smoother with multiple data assimilation. Comput. Geosci. 55, 3–15, Ensemble Kalman filter for data assimilation.

Evensen, G., 1994. Sequential data assimilation with a nonlinear quasi-geostrophic model using Monte Carlo methods to forecast error statistics. J. Geophys. Res. Oceans 99 (C5), 10143–10162.

Evensen, G., van Leeuwen, P.J., 2000. An ensemble Kalman smoother for nonlinear dynamics. Mon. Weather Rev. 128 (6), 1852–1867.

Farrell, B.F., Ioannou, P.J., 2001. State estimation using a reduced-order Kalman filter. J. Atmos. Sci. 58 (23), 3666–3680.

Heemink, A., Mouthaan, E., Roest, M., Vollebregt, E., Robaczewska, K., Verlaan, M., 2002. Inverse 3D shallow water flow modelling of the continental shelf. Cont. Shelf Res. 22 (3), 465–484.

Jolliffe, I., Cadima, J., 2016. Principal component analysis: A review and recent developments. Phil. Trans. R. Soc. A 374, 20150202.

Jongman, B., Ward, P.J., Aerts, J.C., 2012. Global exposure to river and coastal flooding: Long term trends and changes. Global Environ. Change 22 (4), 823–835.

Karri, R.R., Badwe, A., Wang, X., El Serafy, G., Sumihar, J., Babovic, V., Gerritsen, H., 2013. Application of data assimilation for improving forecast of water levels and residual currents in Singapore regional waters. Ocean Dyn. 63 (1), 43–61.

Kernkamp, H., Van Dam, A., Stelling, G., de Goede, E., 2011. Efficient scheme for the shallow water equations on unstructured grids with application to the Continental Shelf. Ocean Dyn. 1–14.

Kopp, G.A., Ferre´, J.A., Giralt, F., 1997. The use of pattern recognition and proper orthogonal decomposition in identifying the structure of fully-developed free turbulence. J. Fluids Eng. 119 (2), 289–296.

Kosambi, D.D., 1943. Statistics in function space. J. Indian Math. Soc. 7, 76–88.

Liang, Y.C., Lee, H.P., Lim, S.P., Lin, W.Z., Lee, K.H., Wu, C.G., 2002. Proper orthogonal decomposition and its applications—part i: Theory. J. Sound Vib. 252 (3), 527–544. http://dx.doi.org/10.1006/jsvi.2001.4041.

Lin, B., McLaughlin, D., 2014. Efficient characterization of uncertain model parameters with a reduced-order ensemble Kalman filter. SIAM J. Sci. Comput. 36 (2), B198–B224.

Lumley, J.L., 1967. The structure of inhomogeneous turbulence. In: Atmospheric Turbulence and Radio Propagation. pp. 166–178.

Lyard, F.H., Allain, D.J., Cancet, M., Carrère, L., Picot, N., 2021. FES2014 global ocean tide atlas: design and performance. Ocean Sci. 17 (3), 615–649. http://dx.doi.org/10.5194/os-17-615-2021, URL: https://os.copernicus.org/articles/17/615/2021/.

Mahfouf, J.-F., Rabier, F., 2000. The ECMWF operational implementation of four-dimensional variational assimilation. II: Experimental results with improved physics. Q. J. R. Meteorol. Soc. 126 (564), 1171–1190.

Maraldi, C., Lyard, F., Testut, L., Coleman, R., 2011. Energetics of internal tides around the Kerguelen Plateau from modeling and altimetry. J. Geophys. Res. Oceans 116 (C6).

Mayo, T., Butler, T., Dawson, C.N., Hoteit, I., 2014. Data assimilation within the advanced circulation (ADCIRC) modeling framework for the estimation of Manning's friction coefficient. Ocean Model..

Monahan, A.H., Fyfe, J.C., Ambaum, M.H.P., Stephenson, D.B., North, G.R., 2009. Empirical orthogonal functions: The medium is the message. J. Clim. 22 (24), 6501–6514.

Muis, S., Verlaan, M., Nicholls, R.J., Brown, S., Hinkel, J., Lincke, D., Vafeidis, A.T., Scussolini, P., Winsemius, H.C., Ward, P.J., 2017. A comparison of two global datasets of extreme sea levels and resulting flood exposure. Earth's Future 5 (4), 379–392.

Ngodock, H.E., Souopgui, I., Wallcraft, A.J., Richman, J.G., Shriver, J.F., Arbic, B.K., 2016. On improving the accuracy of the M2 barotropic tides embedded in a high-resolution global ocean circulation model. Ocean Model. 97, 16–26. http://dx.doi.org/10.1016/j.ocemod.2015.10.011, URL: https://www.sciencedirect.com/science/article/pii/S1463500315002140.

Pringle, W.J., Wirasaet, D., Roberts, K.J., Westerink, J.J., 2021. Global storm tide modeling with ADCIRC v55: unstructured mesh design and performance. Geosci. Model Dev. 14 (2), 1125–1145. http://dx.doi.org/10.5194/gmd-14-1125-2021, URL: https://gmd.copernicus.org/articles/14/1125/2021/.

Pugh, D., 1996. Tides, Surges and Mean Sea-Level. John Wiley & Sons, Ltd..

Pugh, D., Woodworth, P., 2014. Sea-Level Science: Understanding Tides, Surges, Tsunamis and Mean Sea-Level Changes. Cambridge University Press.

Ralston, M.L., Jennrich, R.I., 1978. Dud, a derivative-free algorithm for nonlinear least squares. Technometrics 20 (1), 7–14.

Stammer, D., Ray, R.D., Andersen, O.B., Arbic, B.K., Bosch, W., Carrère, L., Cheng, Y., Chinn, D.S., Dushaw, B.D., Egbert, G.D., Erofeeva, S.Y., Fok, H.S., Green, J.A.M., Griffiths, S., King, M.A., Lapin, V., Lemoine, F.G., Luthcke, S.B., Lyard, F., Morison, J., Müller, M., Padman, L., Richman, J.G., Shriver, J.F., Shum, C.K., Taguchi, E., Yi, Y., 2014. Accuracy assessment of global barotropic ocean tide models. Rev. Geophys. 52 (3), 243–282.

Tozer, B., Sandwell, D.T., Smith, W.H.F., Olson, C., Beale, J.R., Wessel, P., 2019. Global bathymetry and topography at 15 arc sec: SRTM15+. Earth Space Sci. 6 (10), 1847–1864.

Trémolet, Y., 2007. Incremental 4D-var convergence study. Tellus A 59 (5), 706–718.

Verlaan, M., De Kleermaeker, S., Buckman, L., 2015. GLOSSIS: Global storm surge forecasting and information system [online]. In: Australasian Coasts & Ports Conference 2015: 22nd Australasian Coastal and Ocean Engineering Conference and the 15th Australasian Port and Harbour Conference. Engineers Australia and IPENZ, Auckland, New Zealand, pp. 229–234.

Wang, X., Verlaan, M., Apecechea, M.I., Lin, H.X., 2021. Computation-efficient parameter estimation for a high-resolution global tide and surge model. J. Geophys. Res. Oceans 126 (3), e2020JC016917.

Ward, P., Jongman, B., Salamon, P., Simpson, A., Bates, P., de Groeve, T., Muis, S., Coughlan, E., Rudari, R., Trigg, M., Winsemius, H., 2015. Usefulness and limitations of global flood risk models. Nature Clim. Change 5, 712–715. http://dx.doi.org/10.1038/nclimate2742.

Weatherall, P., Marks, K.M., Jakobsson, M., Schmitt, T., Tani, S., Arndt, J.E., Rovere, M., Chayes, D., Ferrini, V., Wigley, R., 2015. A new digital bathymetric model of the world's oceans. Earth Space Sci. 2 (8), 331–345.

Zaron, E.D., 2019. Simultaneous estimation of ocean tides and underwater topography in the weddell sea. J. Geophys. Res. Oceans 124 (5), 3125–3148.

Zijl, F., Verlaan, M., Gerritsen, H., 2013. Improved water-level forecasting for the Northwest European Shelf and North Sea through direct modelling of tide, surge and non-linear interaction. Ocean Dyn. 63 (7), 823–847.